

RGS-DR: Reflective Gaussian Surfels with Deferred Rendering for Shiny Objects

Georgios Kouros Minye Wu Tinne Tuytelaars
 KU Leuven

{georgios.kouros,minye.wu,tinne.tuytelaars}@esat.kuleuven.be

Abstract

We introduce RGS-DR, a novel inverse rendering method for reconstructing and rendering glossy and reflective objects with support for flexible relighting and scene editing. Unlike existing methods (e.g., NeRF and 3D Gaussian Splatting), which struggle with view-dependent effects, RGS-DR utilizes a 2D Gaussian surfel representation to accurately estimate geometry and surface normals, an essential property for high-quality inverse rendering. Our approach explicitly models geometric and material properties through learnable primitives rasterized into a deferred shading pipeline, effectively reducing rendering artifacts and preserving sharp reflections. By employing a multi-level cube mipmap, RGS-DR accurately approximates environment lighting integrals, facilitating high-quality reconstruction and relighting. A residual pass with spherical-mipmap-based directional encoding further refines the appearance modeling. Experiments demonstrate that RGS-DR achieves high-quality reconstruction and rendering quality for shiny objects, often outperforming reconstruction-exclusive state-of-the-art methods incapable of relighting.

1. Introduction

Reconstructing and rendering glossy and reflective objects remain significant challenges in computer vision and graphics. These objects exhibit strong view-dependent effects, such as specular highlights and reflections, which undermine multi-view consistency and increase the difficulty of recovering accurate 3D geometry and appearance from multi-view images. In real-world scenarios, such objects are prevalent, including automobiles, metallic artifacts, and ceramic tableware. Achieving high-quality reconstruction and rendering of such surfaces is crucial for enhancing realism and user immersion in applications such as virtual reality (VR), augmented reality (AR), and gaming.

Recent advances in novel view synthesis (NVS) methods have demonstrated high-fidelity scene reconstruction and rendering quality when applied to objects with predominantly Lambertian reflectance. However, state-of-the-art



Figure 1. RGS-DR delivers high-quality inverse rendering by disentangling scene geometry, material properties, and illumination, enabling photorealistic rendering, relighting, and scene editing.

techniques such as Neural Radiance Fields (NeRF) [23] and 3D Gaussian Splatting [15] struggle to achieve satisfactory results on glossy and reflective surfaces. The primary limitation arises from their lack of explicit modeling of light transport. These methods rely heavily on multi-view consistency, which fails to capture sufficient cues for reconstructing complex specular effects. Consequently, artifacts such as blurring and floating structures (floaters) frequently occur.

To address these issues, inverse neural rendering aims to decompose scene properties and approximate light transport. Techniques in this area [12, 16, 33] have led to significant improvements in rendering shiny objects. A core component of these methods is the estimation of reflection directions based on surface normals, which is essential for modeling specular reflections under environmental lighting. The quality of reconstruction and rendering is highly dependent on the accuracy of these surface normals. To obtain them, Ref-NeRF [33] uses multilayer perceptrons to learn coordinate-based normals, while GaussianShader [12] employs learnable normal residuals conditioned on the viewing direction. However, both methods detach the normal estimation from the underlying geometry, which may result in noisy normals. Other methods, such as NMF [21] and ENVIDR [17], achieve better performance by using normals

derived from the gradient of the geometry, while 3DGS-DR [16] relies on the shortest axis of each Gaussian ellipsoid to estimate normals that may or may not align with the actual surface of the object. In contrast, Ref-GS [39] takes advantage of standard surfel modeling [25], adopting 2D-oriented disks as surface elements, providing an explicit normal representation that enhances the modeling of shiny objects. However, Ref-GS encodes some of the object’s material properties implicitly together with the ambient lighting, making it difficult to edit the scene, such as changing the environment lighting.

To achieve relighting with inverse rendering, it is essential to explicitly model the environment lighting within the rendering equation. This explicit modeling enables the seamless replacement of the original lighting with the desired target lighting for effective relighting. Existing methods approximate the rendering equation using different formulations to enable this explicit modeling. A key challenge in this process is the accurate modeling of the integral of incident light from different directions. Spherical Harmonics [21] and Spherical Gaussians [33, 37] are commonly used to represent the distribution of environment lighting, as they provide closed-form solutions for approximating light integration. Other methods [12, 16, 39] utilize discrete grid textures to capture high-frequency signals in environment lighting. However, 3DGS-DR [16], the state-of-the-art method in this domain, fails to properly formulate the integral using only a single-level environment map, which limits its expressive capability. Meanwhile, GaussianShader [12], which samples from multi-level mipmaps to approximate the integral, struggles with geometric uncertainty, resulting in degraded results.

In this paper, we introduce *RGS-DR*, a method that enables high quality shiny object reconstruction and rendering, while supporting scene relighting. *RGS-DR* inherits the surfel representation from 2DGS [11], enabling accurate geometry modeling and surface normal computation. We decompose the scene’s geometric and material properties and store them as learnable variables within each 2D Gaussian primitive. In the proposed rendering pipeline, the properties of these Gaussians are rasterized to generate a material property buffer in image space. We use a deferred rendering method, applying shading functions to each pixel in the graphics buffer to determine its final color. This approach mitigates the impact of depth precision on rendering and prevents the degradation of rendering quality due to the accumulation of geometric errors and uncertainties during alpha blending - an issue commonly found in traditional methods. In these shading functions, the light transport is considered, and the environment map is explicitly modeled using mip-mapping. We use a multi-level cube-map structure that enhances the accuracy of the light integral approximation on a discrete grid. We also model

inter-reflections as a residual in a deferred rendering formulation and incorporate a residual pass that includes the spherical encoding from Ref-GS [39] that further enhances the rendering quality. Additionally, our method produces relighting effects by replacing the content of the explicit environment map, while modifying the Gaussians’ material attributes—such as roughness and diffuse color—unlocks scene editing capabilities. Experimental results show that *RGS-DR* achieves high reconstruction quality, on par with state-of-the-art reconstruction-only techniques, while also providing plausible estimates of the environment illumination and the material properties of the scene.

2. Related Work

Novel View Synthesis. Neural Radiance Fields (NeRF) [22] offer an end-to-end framework for synthesizing photorealistic images from sets of 2D images using implicit neural representations. While NeRF offers high photorealism and compact representation, it is inefficient in training and rendering. To address this, subsequent approaches have incorporated hybrid implicit-explicit representations, such as voxel grids [18, 28, 30, 31] and hash encodings [24], which significantly enhance computational efficiency without compromising reconstruction quality. However, these methods face challenges when dealing with shiny objects due to geometric ambiguities arising from multi-view inconsistencies and their stochastic geometry modeling.

3D Gaussian Splatting (3DGS) [15] has recently emerged as a promising alternative to NeRF for 3D scene representation, delivering high-quality novel view synthesis and rapid rendering speeds. Advancements in 3DGS, such as the use of structured Gaussians [6, 20, 26], texture mapping [5], gradient cues [27, 40], and anti-aliasing [36], have further enhanced rendering quality. However, these methods often fall short in accurately reconstructing and rendering glossy or reflective surfaces due to their inability to precisely model surface-light interactions. To address these limitations, 2D Gaussian Splatting (2DGS) [11] projects Gaussian disks onto object surfaces and applies local smoothing. This approach ensures view-consistent geometry. Our method leverages its explicit surface normals combined with a tailored shading function to accurately model light transport in scenes featuring shiny objects.

Inverse Neural Rendering. Inverse rendering is a challenging problem that seeks to reconstruct scene properties, including geometry, materials, and lighting, from images. Recent advances in inverse rendering have integrated differentiable volume rendering with implicit neural representations, drawing inspiration from NeRF [22], to learn scene representations encompassing both geometry and materials. Early approaches in this area often made strong assumptions or required additional priors, such as a known illumina-

nation [2, 29], geometry [38], or varying illumination conditions [2, 10]. These limitations have been addressed in subsequent works [3, 4, 9, 13, 17, 33, 37], which jointly estimate geometry, materials (e.g., BRDF), and lighting. Gaussian-based neural rendering methods [12, 32, 35, 41] provide faster solutions. These studies calculate reflection directions to model light transport, thereby achieving superior performance compared to traditional neural rendering methods when handling shiny objects. Recent works [16, 39] on this task employ deferred rendering [8] on material buffer images. Our method inherits the deferred rendering scheme and explicitly models both the material properties and environment map without relying on alpha blending. This approach produces sharp reflection effects and facilitates property editing, as illustrated in Fig. 1.

3. Preliminary

2D Gaussian Splatting [11] projects 3D Gaussians [15] onto 2D oriented planar disks, ensuring view-consistent geometry and explicit normals, defined as the direction of the steepest density change. Each planar disk serves as a 2D Gaussian primitive, characterized by a center point \mathbf{x} , two principal tangential vectors \mathbf{t}_u and \mathbf{t}_v , and two variance-controlling scaling factors s_u and s_v that need to be optimized. We use the covariance matrix Σ to represent the rotation and scaling of each gaussian. Instead of evaluating Gaussian values at the intersection of a pixel ray and a 3D Gaussian, 2DGS computes them directly on 2D disks, leveraging explicit ray-splat intersections for perspective-correct splatting. The Gaussian value is formulated as: $\mathcal{G}(\mathbf{u}(\mathbf{r})) = \exp(-(u^2 + v^2)/2)$, where $\mathbf{u}(\mathbf{r}) = (u, v)$ is the intersection point between ray \mathbf{r} and the disk in UV space.

For rendering, Gaussians along with their properties, such as color \mathbf{c}_i , are sorted by their centers and blended into pixels front to back, which is formulated by alpha blending:

$$c(\mathbf{r}) = \sum_{i=1}^n \mathbf{c}_i \alpha_i \mathcal{G}_i(\mathbf{u}(\mathbf{r})) \prod_{j=1}^{i-1} (1 - \alpha_j \mathcal{G}_j(\mathbf{u}(\mathbf{r}))), \quad (1)$$

where i and α_i denote the index of the Gaussian and its alpha value; \mathbf{c}_i is the view-dependent appearance color for the i -th Gaussian. In our method, we need to render different object material properties (e.g. diffuse color, roughness, and normal) and feature vectors into the target view. This is achieved using alpha blending, where the principle is to replace the color \mathbf{c}_i with the corresponding material properties or features, generating multi-channel pixel values.

Planar disks have well-defined surface normals that are perpendicular to their surfaces. Using the tangential vectors, we can compute the normal vectors in closed form:

$$\mathbf{n} = \mathbf{t}_u \times \mathbf{t}_v, \quad (2)$$

where \mathbf{n} is the normal vector, and operator \times stands for cross product. In our method, we use this explicit normal formulation in the light transport modeling, enabling accurate reflection calculations. This perspective-correct rendering improves the performance rendering based on deferred shading.

4. Methodology

RGS-DR exploits surfel primitives that have accurate surface properties to compose the scene. In addition to the geometry-related variables mentioned above, each primitive has learnable properties, namely diffuse color \mathbf{c}_d , roughness ρ , and specular tint \mathbf{s} . We also assign a feature vector \mathbf{f} to each primitive to capture inter-reflection.

Overview. Instead of first calculating the view-dependent color of primitives and then blending them, we employ a deferred rendering scheme. Our approach rasterizes the geometry and blends the properties into a Graphics Buffer (G-Buffer), which stores buffer images for each property (§ 4.1). The G-Buffer stores essential information for modeling light transport in reflections, including geometry, material, and lighting-related properties. It enables a representation of global illumination effects. Leveraging this data, shading functions are applied to approximate the rendering equation based on the material attributes in the G-Buffer. This process enables the computation of pixel-wise colors for the specular component while accounting for indirect lighting contributions from surrounding environment (§ 4.2). In addition to environmental illumination, light undergoes multiple reflections between object surfaces, a phenomenon known as inter-reflection, which is not explicitly modeled in standard shading functions. To address this limitation, we propose a residual rendering pass that integrates features from the G-Buffer with a spherical feature mip-map [] to effectively encode inter-reflection effects (§ 4.3). We integrate these components into our proposed differentiable pipeline to generate the final rendered images. The complete pipeline is illustrated in Fig. 2.

Deferred Rendering. RGS-DR approximates the rendering equation with:

$$\mathbf{c}(\omega_o) = \mathbf{c}_d + \mathbf{s} \odot \mathbf{L}_s(\omega_o, \mathbf{n}, \rho) + \mathbf{c}_r(\omega_o), \quad (3)$$

where $\omega_o \in \mathbb{R}^3$ is the viewing direction, $\mathbf{c}_d \in \mathbb{R}^3$ is the diffuse color, $\mathbf{s} \in \mathbb{R}^3$ is the specular tint, $\mathbf{L}_s \in \mathbb{R}^3$ is the specular light from the shading functions (§ 4.2), $\rho \in \mathbb{R}^1$ is the roughness, and $\mathbf{c}_r \in \mathbb{R}^3$ is a residual color term (§ 4.3) that accounts for inter-reflection effects. Note that deferred rendering computes on the image pixel level; all the input variables are fetched from the G-buffer at the corresponding pixel coordinates. The final rendered image \mathcal{I} is calculated as

$$\mathcal{I} = \mathcal{I}_d + \mathcal{I}_s + \mathcal{I}_r, \quad (4)$$

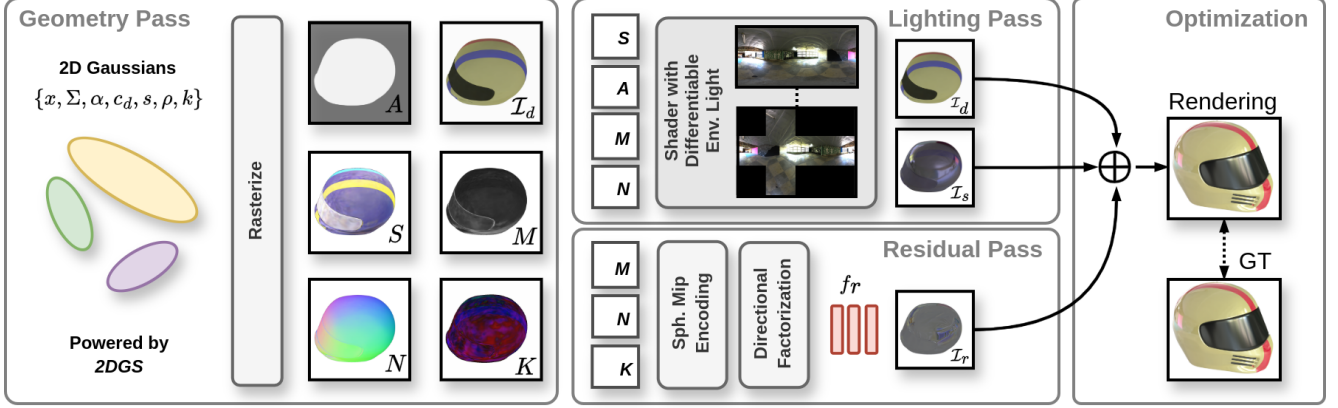


Figure 2. Our rendering pipeline consists of three passes. The geometry pass produces screen-space diffuse color \mathcal{I}_d , specular tint S , roughness M , normals N , and low-dimensional features K , which feed into the subsequent passes. The lighting pass employs a cube mipmap to model environmental light for shading as described in [12]. Meanwhile, the residual pass uses a spherical-mip-based directional encoding (inspired by [39]) along with a shallow MLP f_r to predict view-dependent effects not captured by the lighting pass.

where \mathcal{I}_d and \mathcal{I}_s are the diffuse and specular components of the scene, while \mathcal{I}_r is the residual image term. The components of Eq. 3-4 will be introduced in the following subsections.

4.1. G-Buffer Rendering

We adapt the alpha blending formulation in Eq. 1 to generate buffer images by replacing c_i with the corresponding property vectors. RGS-DR fills the G-buffer with the diffuse map \mathcal{I}_d , roughness map M , specular tint map S , feature map K , and normal map N , as well as the accumulated alpha map A . They have the same resolution as the render target's but differ in the number of channels. Most of them are alpha-blended from corresponding properties stored in each Gaussian primitive except for the normal map N , which is derived from the primitive geometry using Eq. 2. Given a specific pixel coordinate, the desired property at that location can be obtained by interpolating the corresponding values from the buffer image.

4.2. Deferred Shading Functions

Shading functions are an important part of the approximation of the rendering equation [14] to model light-surface interactions. They have been used in [12], demonstrating their effectiveness in material decomposition and representation. In this work, we extend shading functions to the deferred rendering framework and apply them to the G-buffer.

We use a shading function to compute the specular component L_s , which is formulated as:

$$L_s(\omega_o, \mathbf{n}, \rho) = \int_{\Omega} L(\omega_i) D(\omega_r, \rho) (\omega_i \cdot \mathbf{n}) d\omega_i, \quad (5)$$

where Ω denotes the directions of the entire upper hemisphere above the current primitive disk, and D is the

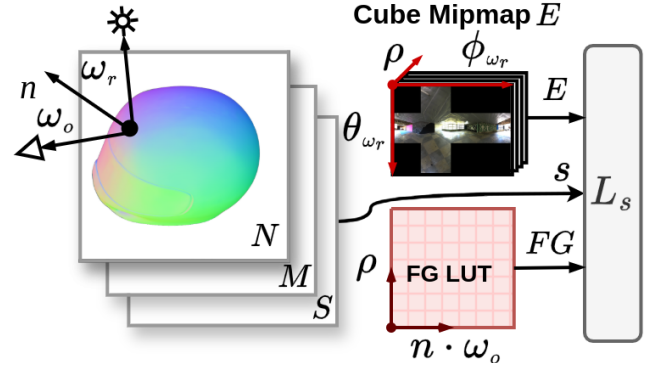


Figure 3. Specular light computation for the lighting pass using a differentiable environment light encoded as a cube mipmap.

GGX [34] normal distribution function; ω_i is the direction of the input radiance.

The integration is approximated using the split-sum approximation to avoid computationally expensive explicit integral evaluations. Specifically, we achieve this using a pre-filtered cube mip-map \mathbf{E} where each mip-map level stores progressively blurrier versions of the original environment map, simulating different levels of surface roughness for reflections. Paired with a Look-Up Table F for Fresnel and Geometric terms [7] that modulates specular reflections, we approximate the integral calculation using following formulation:

$$L_s(\omega_o, \mathbf{n}, \rho) = \mathbf{s} \cdot F(\mathbf{s}, \rho, \mathbf{n}, \omega_o) \cdot \Phi(\omega_r, \rho, \mathbf{E}) + (1 - \mathbf{s}) \cdot \Phi(\omega_r, \rho_0, \mathbf{E}), \quad (6)$$

where the reflection direction is given by $\omega_r = 2(\omega_o \cdot \mathbf{n})\mathbf{n} - \omega_o$. The function $\Phi(\cdot)$ samples the mip-map \mathbf{E} at a specific level determined by the input roughness. Here, ρ_0 represents a high roughness value. Consequently, $\Phi(\omega_r, \rho_0, \mathbf{E})$

characterizes the ambient lighting from the environment. It enhances the low-frequency reflection. Figure 3 illustrates the pipeline of computing \mathbf{L}_s .

In contrast to GaussianShader [12] which applies shading on each individual 3D Gaussian before splatting, we defer shading and apply it at the pixel level. This approach provides two benefits. First, we compute lighting only on the visible parts of the scene, and second, we leverage the smooth normals that are produced from 2D Gaussian primitive, which are far more accurate than the shortest normal axes of 3D Gaussians. At the same time, we do not have to learn additional normal residuals as does GaussianShader to account for inconsistencies between surface normals and Gaussian normals. In the deferred rendering scheme, pixel shading is performed without alpha blending, resulting in high-frequency reflections.

4.3. Residual Rendering Pass

We incorporate a residual color term optimized in what we call the residual pass, as shown in Fig.2. Instead of using high-dimensional spherical harmonic coefficients per Gaussian, we employ low-dimensional features \mathbf{k} and optimize a directional encoding based on the methodology of Ref-GS [39]. This involves a spherical mipmap-based directional encoding that enables roughness-aware photorealistic rendering on highly reflective scenes. However, the environment illumination in Ref-GS is baked in the mipmap, and thus learned scenes are not relightable. Instead, we leverage the high expressivity of such a directional encoding to learn scene-specific information and augment the reconstruction quality of our model. The resulting residual color term complements our explicit shading branch and accounts for missing complex view-dependent effects, such as inter-reflections, thus refining our method’s reconstruction quality. However, relighting quality is not affected as the residual term is illumination-specific and is not included when performing relighting by rendering with new environment maps.

For a given screen-space point $\mathbf{u}(u, v)$, the spherical mip encoding can be calculated based on the viewing direction ω_o , normal \mathbf{n} , roughness ρ , and feature \mathbf{k} . The viewing direction and normal are used to estimate the reflected direction ω_r which is then converted into polar coordinate (θ_r, ϕ_r) . The spherical mip encoding is then computed by trilinear interpolation on the spherical mipmap \mathcal{M} along the roughness dimension and given by $\mathbf{h} = \text{Sph-Mip}(\omega_r, \rho, \mathcal{M})$. This feature is concatenated with the outer product $\mathbf{h} \otimes \mathbf{k}$ to form the directional encoding, which is used as input to a shallow MLP f_r to produce the residual color term $\mathbf{c}_r = f_r(\mathbf{h}, \mathbf{k} \otimes \mathbf{h})$ and the corresponding residual image

$$\mathcal{I}_r = f_r(\mathbf{H}, \mathbf{K} \otimes \mathbf{H}). \quad (7)$$

4.4. Training Strategy

To train our model, we follow the training strategy of 3DGS [15], which supervises the model with a photometric RGB reconstruction loss \mathcal{L}_c that combines an \mathcal{L}_1 loss with a D-SSIM term into

$$\mathcal{L}_c = (1 - \lambda) \mathcal{L}_1 + \lambda \mathcal{L}_{\text{D-SSIM}}, \quad (8)$$

where λ is the balancing term between the two losses and is usually chosen as $\lambda = 0.2$.

However, the problem of estimating 3D geometry from a collection of posed 2D images using only a photometric loss is ill-posed. As a result, we additionally adopt the regularization methodology of 2DGS [11]. This regularization involves the normal consistency regularization from Ref-NeRF [33], given in Eq. 9 and the depth distortion regularization from MipNeRF360 [1], given in eq. 10. The former tries to enforce consistency between the predicted normal map and the normals computed by depth gradients and is formulated as

$$\mathcal{L}_n = \sum_i w_i (1 - \mathbf{n}_i^T \mathbf{N}), \quad (9)$$

where i , w_i , \mathbf{n}_i , and N correspond to a ray-splat intersection, its blending weight, its normal, and the local depth normal calculated using finite differences from nearby depth points. The latter regularizes the weight distribution of the splats to concentrate them around the surface by minimizing the surface-splat intersection. This is accomplished through

$$\mathcal{L}_d = \sum_{i,j} w_i w_j |z_i - z_j|, \quad (10)$$

where z_i is the depth of the i -th ray-splat intersection.

Furthermore, we use an alpha loss to prevent floaters caused by redundant Gaussians:

$$\mathcal{L}_\alpha = \|\hat{A} - A\|_1, \quad (11)$$

where \hat{A} is the accumulated alpha map in the G-buffer and A is the corresponding ground-truth alpha channel of the provided RGBA image.

The total loss is calculated as a weighted sum of the individual loss terms as

$$\mathcal{L} = \mathcal{L}_c + \lambda_d \mathcal{L}_d + \lambda_n \mathcal{L}_n + \lambda_\alpha \mathcal{L}_\alpha, \quad (12)$$

where λ_d is the weight of the depth distortion loss, λ_n is the weight of the normal consistency loss and λ_α is the weight of the silhouette loss.

5. Experimental Results

5.1. Datasets

Our method is evaluated against state-of-the-art methods on two popular synthetic datasets with complex view-

dependent effects due to highly reflective surfaces. Specifically, we evaluate on the Shiny Blender, Shiny Real [33], and Glossy Synthetic [19]. Results are provided for all scenes in the Shiny Synthetic and Shiny Real datasets. For the Glossy Synthetic dataset, we select the same subset of scenes as in [16, 39].

5.2. Implementation Details

All our models are trained on an NVIDIA Tesla P100 GPU (16GB VRAM), completing 35k iterations in roughly two hours. For the lighting pass, we use a cube mipmap of size $6 \times 512 \times 512$ with 3 RGB channels, and for the residual pass an $8 \times 512 \times 512$ mipmap with 16 feature channels, along with a shallow MLP (two hidden layers of 256 units). For the real scenes, we downsample the training images of the gardenspheres and toy car scenes by factors of 4 and the sedan scene by a factor of 8 to be consistent with 3DGS-DR [16]. Furthermore, we employ a similar bounding volume as in [16] to allow for reflective surfaces only in the foreground object and penalize reflective surfels in the background. We achieve this by penalizing low roughness properties in Gaussians outside of the bounding volume. Loss weights are set as follows: normal consistency loss ($\lambda_n = 0.05$) begins at 5k iterations, depth distortion loss ($\lambda_d = 100$) at 3k iterations, and alpha loss ($\lambda_\alpha = 1.0$) from the start—downweighted by a factor of 0.8 at 7k iterations. Material properties (diffuse color, roughness, tint) are optimized at a learning rate of 2.5×10^{-3} , while opacity, scaling, and rotation use rates of 0.03, 3×10^{-3} , and 10^{-2} , respectively. The environment cube mipmap follows an exponential decay from 10^{-2} to 10^{-3} , and the positions of the 2D Gaussian discs are trained following the original 2DGS methodology [11] with a decay from 1.6×10^{-4} to 1.6×10^{-6} . Initially, the model is trained without the residual pass. After 30k iterations, we activate it while freezing the geometry, material properties, and lighting model. At this stage, only the spherical encoding mipmap, MLP weights, and features are updated, so the residual term benefits mainly reconstruction and not relighting.

5.3. Comparison

In Table 1 and Fig. 4, we present the quantitative and qualitative evaluation of our proposed methodology against state-of-the-art novel view synthesis and inverse rendering methods. As shown in the table, we outperform the competing methods on several scenes of the Shiny Synthetic and Shiny Blender datasets. Specifically, our method appears superior on the most glossy objects such as car, helmet, and toaster, as well as the entire Glossy Synthetic dataset. Our results in Fig. 4 highlight the ability of our method to reconstruct sharper reflections with less blurring and distortions than the two main competing inverse rendering methods. Since the authors of Ref-GS [39] have not released the code

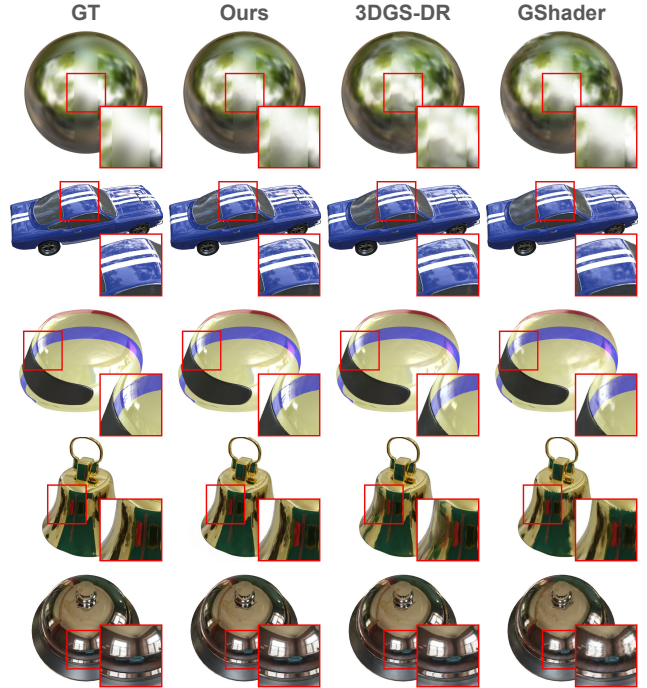


Figure 4. Comparison of the rendering quality of our method against 3DGS-DR [16] and GaussianShader [12].

yet, we cannot compare qualitatively against them, and instead focus on the most relevant inverse rendering methods, namely, 3DGS-DR [16] and GaussianShader [12].

In Fig. 5, we present the decomposition of our method’s output including the material properties, smooth geometry (visualized through surface normals), as well as the estimated specular components and residuals. As demonstrated, our method effectively disentangles the geometry, material properties, and illumination of a given scene, thus enabling photorealistic novel view synthesis, relighting, and scene editing. Unlike 3DGS-DR, our method learns explicit material properties and thus trained scenes can be easily ported to existing 3D rendering engines.

In Fig. 6, we present our method’s estimated environment illumination for four scenes of the Shiny Synthetic dataset. Our method manages to effectively disentangle the illumination from the material properties and geometry of the scene. Compared to 3DGS-DR and GaussianShader, we obtain more refined environment maps with sharper details, fewer artifacts, and closer to the ground truth.

5.4. Ablation Study

In Table 2, we conduct an ablation study to showcase the contributions of our method. First, we replace the cube mipmap of the environment light with a single cubemap to compare with 3DGS-DR that uses a single level. We observe a considerable drop in performance, demonstrating

Table 1. Quantitative results comparing our method with state-of-the-art approaches on test views from the Shiny Synthetic and Glossy Synthetic datasets. Metrics from [16, 39] are used, with the top three methods for each scene and metric marked as **first**, **second**, and **third**. Methods indicated by † do not support relighting. The final columns present the average scores for each dataset.

Datasets	Shiny Synthetic [33]							Glossy Synthetic [19]							Shiny Real [33]			
	ball	car	coffee	helmet	teapot	toaster	avg	bell	cat	luyu	potion	shell	teapot	avg	garden	sedan	toycar	avg
PSNR ↑																		
Ref-NeRF†	33.16	30.44	33.99	29.94	45.12	26.12	33.13	30.02	29.76	25.42	30.11	26.91	22.77	27.50	22.01	25.21	23.65	23.62
3DGS†	27.65	27.26	32.30	28.22	45.71	20.99	30.36	25.11	31.36	26.97	30.16	23.88	21.51	26.50	21.75	26.03	23.78	23.85
GShader	30.99	27.96	32.39	28.32	45.86	26.28	31.97	28.07	31.81	27.18	30.09	24.48	23.58	27.54	21.74	24.89	23.76	23.46
ENVIDR	41.02	27.81	30.57	32.71	42.62	26.03	33.46	30.88	31.04	28.03	32.11	28.64	26.77	29.58	21.47	24.61	22.92	23.00
3DGS-DR	33.66	30.39	34.65	31.69	47.12	27.02	34.09	31.65	33.86	28.71	32.79	28.94	25.36	30.22	21.82	26.32	23.83	23.99
Ref-GS†	36.10	30.94	34.38	33.40	46.69	27.28	34.80	31.70	33.15	29.46	32.64	30.08	26.47	30.58	22.48	26.63	24.20	24.44
Ours	37.76	31.05	33.06	33.97	45.19	27.54	34.76	32.15	32.95	29.74	33.10	30.54	26.61	30.85	23.19	26.25	24.45	24.63
SSIM ↑																		
Ref-NeRF†	0.971	0.950	0.972	0.954	0.995	0.921	0.961	0.941	0.944	0.901	0.933	0.947	0.897	0.927	0.584	0.720	0.633	0.646
3DGS†	0.937	0.931	0.972	0.951	0.996	0.894	0.947	0.892	0.959	0.916	0.938	0.908	0.881	0.916	0.571	0.771	0.637	0.660
GShader	0.966	0.932	0.971	0.951	0.996	0.929	0.958	0.919	0.961	0.914	0.938	0.898	0.901	0.922	0.576	0.728	0.637	0.647
ENVIDR	0.997	0.943	0.962	0.987	0.995	0.990	0.979	0.954	0.965	0.931	0.960	0.947	0.957	0.952	0.561	0.707	0.549	0.606
3DGS-DR	0.979	0.962	0.976	0.971	0.997	0.943	0.971	0.962	0.976	0.936	0.957	0.952	0.936	0.953	0.581	0.773	0.639	0.664
Ref-GS†	0.981	0.961	0.973	0.975	0.997	0.950	0.973	0.965	0.973	0.946	0.957	0.956	0.944	0.957	0.507	0.783	0.682	0.657
Ours	0.988	0.967	0.971	0.977	0.997	0.946	0.974	0.964	0.973	0.952	0.964	0.969	0.951	0.962	0.638	0.769	0.687	0.698
LPIPS ↓																		
Ref-NeRF†	0.166	0.050	0.082	0.086	0.012	0.083	0.080	0.102	0.104	0.098	0.084	0.114	0.098	0.100	0.251	0.234	0.231	0.239
3DGS†	0.162	0.047	0.079	0.081	0.008	0.125	0.084	0.104	0.062	0.064	0.093	0.125	0.102	0.092	0.248	0.206	0.237	0.230
GShader	0.121	0.044	0.078	0.074	0.007	0.079	0.067	0.098	0.056	0.064	0.088	0.122	0.091	0.087	0.274	0.259	0.239	0.257
ENVIDR	0.020	0.046	0.083	0.036	0.009	0.081	0.046	0.054	0.049	0.059	0.072	0.069	0.041	0.057	0.263	0.387	0.345	0.332
3DGS-DR	0.098	0.033	0.076	0.049	0.005	0.081	0.057	0.064	0.040	0.053	0.075	0.067	0.067	0.061	0.247	0.208	0.231	0.229
Ref-GS†	0.098	0.034	0.082	0.045	0.006	0.070	0.056	0.049	0.041	0.046	0.076	0.073	0.064	0.058	0.242	0.196	0.236	0.225
Ours	0.080	0.032	0.084	0.050	0.010	0.097	0.059	0.060	0.038	0.042	0.057	0.049	0.050	0.049	0.264	0.225	0.263	0.251



Figure 5. Outputs of our model including renderings, material properties, residuals and surface normals for scenes from the Shiny Synthetic and Glossy Synthetic datasets. The residuals are amplified for visualization purposes.

Table 2. Ablation study on the Shiny Synthetic [33] dataset.

	PSNR↑	SSIM↑	LPIPS↓
w/o mipmap	33.89	0.968	0.068
w/o residual	34.28	0.974	0.058
Ours	34.76	0.974	0.059

the necessity of a multi-resolution cubemap for accurate estimates of environment illumination. Second, we ablate the residual pass and once again notice a drop in performance, which highlights its benefit to photorealistic reconstruction.

5.5. Relighting and Scene Editing

In Fig. 7, we present the relighting capabilities of our model for three scenes from the Shiny Synthetic dataset [33] and three scenes from the Glossy Synthetic dataset [19]. To relight the scenes, we apply gamma tonemapping to the new environment maps, replace the learned environment map, and convert them to a cube mipmap before rendering. As demonstrated, our method can effectively relight learned scenes and achieve photorealistic results even under new illuminations.



Figure 6. Estimated environment maps for four synthetic scenes from our method RGS-DR, 3DGS-DR [16] and GaussianShader [12].



Figure 7. Relighted scenes. The first column displays the original rendered images while the subsequent columns show relighted scenes with their corresponding environment maps above.

In Fig. 8, on the other hand, we demonstrate the scene editing capabilities of our model on three glossy objects. Specifically, we apply roughness and diffuse editing to make the objects more or less reflective or change their diffuse color.

6. Conclusion

This work addresses the challenges of reconstructing and performing inverse rendering on glossy objects exhibiting intricate geometries and complex view-dependent effects. Our RGS-DR leverages 2D Gaussian Splatting to efficiently achieve precise geometric reconstruction while simultaneously optimizing material properties and scene illumina-



Figure 8. Scene editing: from left to right, the original rendering is followed by versions with decreased roughness, increased roughness, and a modified diffuse color.

tion. By introducing a new deferred shading paradigm that merges a conventional deferred lighting pass with a residual pass to fill in missing details, we significantly enhance the reconstruction quality, achieving performance on par with—and often surpassing—methods dedicated exclusively to reconstruction. Extensive experiments on challenging datasets featuring highly reflective objects demonstrate that our method not only competes with state-of-the-art techniques in reconstruction and inverse rendering, but also delivers high-quality relighting and scene editing.

Acknowledgments

The resources and services used in this work were provided by the VSC (Flemish Supercomputer Center), funded by the Research Foundation - Flanders (FWO) and the Flemish Government.

References

- [1] Jonathan T. Barron, Ben Mildenhall, Dor Verbin, Pratul P. Srinivasan, and Peter Hedman. Mip-nerf 360: Unbounded anti-aliased neural radiance fields. *CVPR*, 2022. 5, 11
- [2] Sai Bi, Zexiang Xu, Kalyan Sunkavalli, Miloš Hašan, Yannick Hold-Geoffroy, David Kriegman, and Ravi Ramamoorthi. Deep reflectance volumes: Relightable reconstructions from multi-view photometric images. In *European Conference on Computer Vision (ECCV)*, page 294–311, Berlin, Heidelberg, 2020. Springer-Verlag. 3
- [3] Mark Boss, Raphael Braun, Varun Jampani, Jonathan T. Barron, Ce Liu, and Hendrik P.A. Lensch. Nerf: Neural reflectance decomposition from image collections. In *IEEE International Conference on Computer Vision (ICCV)*, 2021. 3
- [4] Mark Boss, Varun Jampani, Raphael Braun, Ce Liu, Jonathan T. Barron, and Hendrik P.A. Lensch. Neural-pil: Neural pre-integrated lighting for reflectance decomposition. In *Advances in Neural Information Processing Systems (NeurIPS)*, 2021. 3
- [5] Brian Chao, Hung-Yu Tseng, Lorenzo Porzi, Chen Gao, Tuotuo Li, Qinbo Li, Ayush Saraf, Jia-Bin Huang, Johannes Kopf, Gordon Wetzstein, et al. Textured gaussians for enhanced 3d scene appearance modeling. *arXiv preprint arXiv:2411.18625*, 2024. 2
- [6] Danpeng Chen, Hai Li, Weicai Ye, Yifan Wang, Weijian Xie, Shangjin Zhai, Nan Wang, Haomin Liu, Hujun Bao, and Guofeng Zhang. Pgsr: Planar-based gaussian splatting for efficient and high-fidelity surface reconstruction. *IEEE Transactions on Visualization and Computer Graphics*, 2024. 2
- [7] Robert L Cook and Kenneth E. Torrance. A reflectance model for computer graphics. *ACM Transactions on Graphics (TOG)*, 1(1):7–24, 1982. 4
- [8] Michael Deering, Stephanie Winner, Bic Schediwy, Chris Duffy, and Neil Hunt. The triangle processor and normal vector shader: a vlsi system for high performance graphics. *Acm siggraph computer graphics*, 22(4):21–30, 1988. 3
- [9] Yue Fan, Ivan Skorokhodov, Oleg Voynov, Savva Ignatyev, Evgeny Burnaev, Peter Wonka, and Yiqun Wang. Factored-neus: Reconstructing surfaces, illumination, and materials of possibly glossy objects, 2023. 3
- [10] Duan Gao, Guojun Chen, Yue Dong, Pieter Peers, Kun Xu, and Xin Tong. Deferred neural lighting: free-viewpoint relighting from unstructured photographs. *ACM Transactions on Graphics (TOG)*, 39(6):258, 2020. 3
- [11] Binbin Huang, Zehao Yu, Anpei Chen, Andreas Geiger, and Shenghua Gao. 2d gaussian splatting for geometrically accurate radiance fields. In *SIGGRAPH 2024 Conference Papers*. Association for Computing Machinery, 2024. 2, 3, 5, 6
- [12] Yingwenqi Jiang, Jiadong Tu, Yuan Liu, Xifeng Gao, Xiaoxiao Long, Wenping Wang, and Yuexin Ma. Gaussian-shader: 3d gaussian splatting with shading functions for reflective surfaces. In *Proceedings of the IEEE/CVF Conference on Computer Vision and Pattern Recognition (CVPR)*, pages 5322–5332, 2024. 1, 2, 3, 4, 5, 6, 8, 11, 13, 14
- [13] Haiyan Jin, Isabella Liu, Peijia Xu, Xiaoshuai Zhang, Songfang Han, Sai Bi, Xiaowei Zhou, Zexiang Xu, and Hao Su. Tensor: Tensorial inverse rendering. In *Proceedings of the IEEE/CVF Conference on Computer Vision and Pattern Recognition (CVPR)*, 2023. 3
- [14] James T Kajiya. The rendering equation. In *Proceedings of the 13th annual conference on Computer graphics and interactive techniques*, pages 143–150, 1986. 4
- [15] Bernhard Kerbl, Georgios Kopanas, Thomas Leimkühler, and George Drettakis. 3d gaussian splatting for real-time radiance field rendering. *ACM Transactions on Graphics*, 42(4), 2023. 1, 2, 3, 5
- [16] Ye Keyang, Hou Qiming, and Zhou Kun. 3d gaussian splatting with deferred reflection. 2024. 1, 2, 3, 6, 7, 8, 11, 13, 14
- [17] Ruofan Liang, Huiting Chen, Chunlin Li, Fan Chen, Selvakumar Panneer, and Nandita Vijaykumar. Envidr: Implicit differentiable renderer with neural environment lighting. In *Proceedings of the IEEE/CVF International Conference on Computer Vision*, pages 79–89, 2023. 1, 3
- [18] Lingjie Liu, Jiatao Gu, Kyaw Zaw Lin, Tat-Seng Chua, and Christian Theobalt. Neural sparse voxel fields. *NeurIPS*, 2020. 2
- [19] Yuan Liu, Peng Wang, Cheng Lin, Xiaoxiao Long, Jiepeng Wang, Lingjie Liu, Taku Komura, and Wenping Wang. Nero: Neural geometry and brdf reconstruction of reflective objects from multiview images. *ACM Trans. Graph.*, 42(4), 2023. 6, 7, 11, 12, 14, 16
- [20] Tao Lu, Mulin Yu, Linning Xu, Yuanbo Xiangli, Limin Wang, Dahua Lin, and Bo Dai. Scaffold-gs: Structured 3d gaussians for view-adaptive rendering. In *Proceedings of the IEEE/CVF Conference on Computer Vision and Pattern Recognition*, pages 20654–20664, 2024. 2
- [21] Alexander Mai, Dor Verbin, Falko Kuester, and Sara Fridovich-Keil. Neural microfacet fields for inverse rendering. In *Proceedings of the IEEE/CVF International Conference on Computer Vision*, pages 408–418, 2023. 1, 2
- [22] Ben Mildenhall, Pratul P. Srinivasan, Matthew Tancik, Jonathan T. Barron, Ravi Ramamoorthi, and Ren Ng. Nerf: Representing scenes as neural radiance fields for view synthesis. In *ECCV*, 2020. 2
- [23] Ben Mildenhall, Pratul P Srinivasan, Matthew Tancik, Jonathan T Barron, Ravi Ramamoorthi, and Ren Ng. Nerf: Representing scenes as neural radiance fields for view synthesis. *Communications of the ACM*, 65(1):99–106, 2021. 1
- [24] Thomas Müller, Alex Evans, Christoph Schied, and Alexander Keller. Instant neural graphics primitives with a multiresolution hash encoding. *ACM Trans. Graph.*, 41(4):102:1–102:15, 2022. 2
- [25] Hanspeter Pfister, Matthias Zwicker, Jeroen Van Baar, and Markus Gross. Surfels: Surface elements as rendering primitives. In *Proceedings of the 27th annual conference on Computer graphics and interactive techniques*, pages 335–342, 2000. 2
- [26] Kerui Ren, Lihan Jiang, Tao Lu, Mulin Yu, Linning Xu, Zhangkai Ni, and Bo Dai. Octree-gs: Towards consistent real-time rendering with lod-structured 3d gaussians. *arXiv preprint arXiv:2403.17898*, 2024. 2

- [27] Samuel Rota Bulò, Lorenzo Porzi, and Peter Kotschieder. Revising densification in gaussian splatting. In *European Conference on Computer Vision*, pages 347–362. Springer, 2024. [2](#)
- [28] Sara Fridovich-Keil and Alex Yu, Matthew Tancik, Qinhong Chen, Benjamin Recht, and Angjoo Kanazawa. Plenoxels: Radiance fields without neural networks. In *CVPR*, 2022. [2](#)
- [29] Pratul P. Srinivasan, Boyang Deng, Xiuming Zhang, Matthew Tancik, Ben Mildenhall, and Jonathan T. Barron. Nerv: Neural reflectance and visibility fields for relighting and view synthesis. In *CVPR*, 2021. [3](#)
- [30] Cheng Sun, Min Sun, and Hwann-Tzong Chen. Direct voxel grid optimization: Super-fast convergence for radiance fields reconstruction. In *CVPR*, 2022. [2](#)
- [31] Cheng Sun, Min Sun, and Hwann-Tzong Chen. Improved direct voxel grid optimization for radiance fields reconstruction, 2022. [2](#)
- [32] Zhe Jun Tang and Tat-Jen Cham. 3igs: Factorised tensorial illumination for 3d gaussian splatting. In *European Conference on Computer Vision*, pages 143–159. Springer, 2024. [3](#)
- [33] Dor Verbin, Peter Hedman, Ben Mildenhall, Todd Zickler, Jonathan T. Barron, and Pratul P. Srinivasan. Ref-NeRF: Structured view-dependent appearance for neural radiance fields. *CVPR*, 2022. [1](#), [2](#), [3](#), [5](#), [6](#), [7](#), [11](#), [12](#), [13](#), [15](#)
- [34] Bruce Walter, Stephen R Marschner, Hongsong Li, and Kenneth E Torrance. Microfacet models for refraction through rough surfaces. *Rendering techniques*, 2007:18th, 2007. [4](#)
- [35] Tong Wu, Jia-Mu Sun, Yu-Kun Lai, Yuewen Ma, Leif Kobbelt, and Lin Gao. Deferredgs: Decoupled and editable gaussian splatting with deferred shading. *arXiv preprint arXiv:2404.09412*, 2024. [3](#)
- [36] Zehao Yu, Anpei Chen, Binbin Huang, Torsten Sattler, and Andreas Geiger. Mip-splatting: Alias-free 3d gaussian splatting. In *Proceedings of the IEEE/CVF conference on computer vision and pattern recognition*, pages 19447–19456, 2024. [2](#)
- [37] Kai Zhang, Fujun Luan, Qianqian Wang, Kavita Bala, and Noah Snavely. Physg: Inverse rendering with spherical gaussians for physics-based material editing and relighting. In *Proceedings of the IEEE/CVF Conference on Computer Vision and Pattern Recognition*, pages 5453–5462, 2021. [2](#), [3](#)
- [38] Xiuming Zhang, Pratul P. Srinivasan, Boyang Deng, Paul Debevec, William T. Freeman, and Jonathan T. Barron. Nerfactor: neural factorization of shape and reflectance under an unknown illumination. *ACM Trans. Graph.*, 40(6), 2021. [3](#)
- [39] Youjia Zhang, Anpei Chen, Yumin Wan, Zikai Song, Junqing Yu, Yawei Luo, and Wei Yang. Ref-gs: Directional factorization for 2d gaussian splatting. *arXiv preprint arXiv:2412.00905*, 2024. [2](#), [3](#), [4](#), [5](#), [6](#), [7](#)
- [40] Zheng Zhang, Wenbo Hu, Yixing Lao, Tong He, and Hengshuang Zhao. Pixel-gs: Density control with pixel-aware gradient for 3d gaussian splatting. In *European Conference on Computer Vision*, pages 326–342. Springer, 2024. [2](#)
- [41] Zuo-Liang Zhu, Beibei Wang, and Jian Yang. Gs-ror: 3d gaussian splatting for reflective object relighting via sdf priors. *arXiv preprint arXiv:2406.18544*, 2024. [3](#)

RGS-DR: Reflective Gaussian Surfels with Deferred Rendering for Shiny Objects

Supplementary Material

In this supplementary material, we provide additional qualitative results to showcase the contributions of our proposed methodology, including model outputs and scene decompositions, estimated environment maps, relightings. Last but not least, we provide a video demonstration of our method with smooth animations of rendered scenes showcasing the capabilities of our method for reconstruction, relighting and scene editing. We compare our results with the corresponding results of 3DGS-DR [16] and Gaussian Shader [12] and demonstrate the superiority of our approach.

A. Model Outputs and Scene Properties

In Fig. 9 and Fig. 10, we present the outputs and scene decompositions of our method on the Shiny Synthetic [33] dataset and the Glossy Synthetic [19] dataset, respectively. From left to right, we present the ground-truth color, our method’s reconstructed appearance, diffuse color, specular color, roughness, specular tint, residual color and surface normals. These results demonstrated the capability of our method to effectively disentangle the geometry, material properties and illumination during inverse rendering thus facilitating high quality reconstruction, relighting, and scene editing of reflective surfaces.

B. Recovered Environment Maps

In Fig. 11 and Fig 12 we show additional results on estimated environment maps for all evaluated scenes on the Shiny Synthetic [33] and Glossy Synthetic [19] datasets. As evident, our method consistently outperforms 3DGS-DR [16] and GaussianShader [12], on the shinier scenes e.g. car, helmet and the entire Glossy Synthetic scenes, while being competitive on the rest. In general, we recover sharper details of the environment illumination with less artifacts or blurring, although we note a drop in quality for the rougher objects, e.g. coffee and teapot from the Shiny Synthetic dataset.

C. Additional Relighting Results

In Fig. 13 and Fig. 14, we demonstrate the relighting capabilities of our method by applying three novel environment illuminations on all examined scenes from the two synthetic datasets. We observe high-quality relighted reconstructions with preserved underlying geometry and material properties, while under different lighting.

D. Supplementary Video

In the supplementary video, we demonstrate the outputs of our method using smooth animations of reconstructed scenes. First, we showcase the decomposition of a scene into its material properties and light components (diffuse, specular, residual), as well as the underlying geometry (surface normals). Then we show side-by-side comparisons of rendered objects by our method versus 3DGS-DR [16] and GaussianShader [12]. Our method clearly outperforms both methods on geometry estimation thanks to the utilized 2D Gaussian surfels, showcasing less artifacts, smoother geometry, better appearance reconstruction than GaussianShader and usually on par or better reconstruction than 3DGS-DR. Then we present some additional relighting results before ending the video with more high-quality rendered animations of glossy objects. The video can be watched at the following URL: https://drive.google.com/file/d/1kpqeQsaXWb5cowzXnJSsV_OqOu69zT8G/view?usp=sharing

E. Limitations

Our results reveal several limitations. First, the assumption of deferred shading that each pixel corresponds to the nearest opaque surface prevents proper handling of transparent or refractive objects — a shortcoming that might be overcome by combining deferred rendering for opaque surfaces with forward rendering for transparent ones. Second, the absence of multi-bounce ray tracing and explicit visibility reasoning hinders our ability to manage interreflections and shadows, adversely affecting performance on the coffee and teapot scenes of the Shiny Synthetic dataset [33]. Third, the residual pass is only used for refining the model for novel view synthesis without any benefit to the geometry estimation or relighting tasks. Ideally, the residual should be used to compensate for interreflections and other poorly modelled effects during optimization to alleviate geometry distortions as well. Finally, the approach is not yet applicable to unbounded scenes, requiring either ray contraction [1] and a bounding volume around the foreground object [16] to mitigate interference from sparsely observed background features. Such sparsely seen features in the background are perceived as view-dependent effects that result in erroneous reflective surfels. At the moment, this can only be addressed by using a bounding volume that penalizes low roughness of all surfels outside the bounding volume.

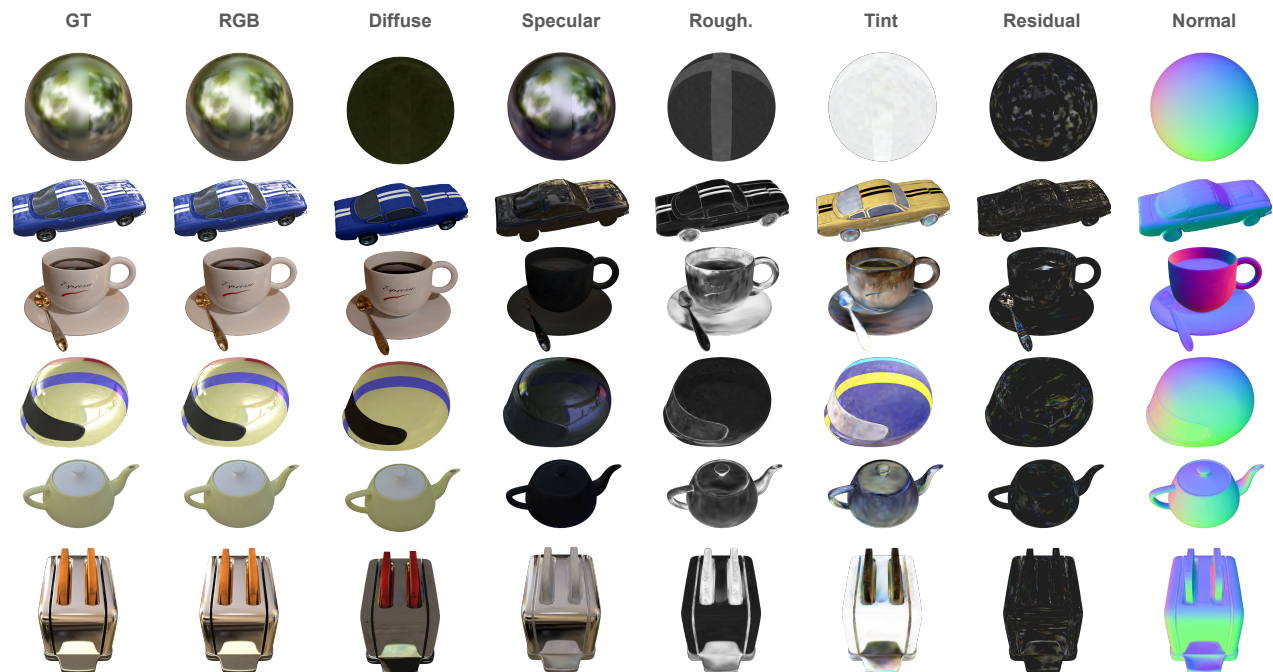


Figure 9. Outputs of our model including diffuse, specular and residual colors, material properties, as well as surface normals for scenes from the Shiny Synthetic [33]. The residuals are amplified for visualization purposes.

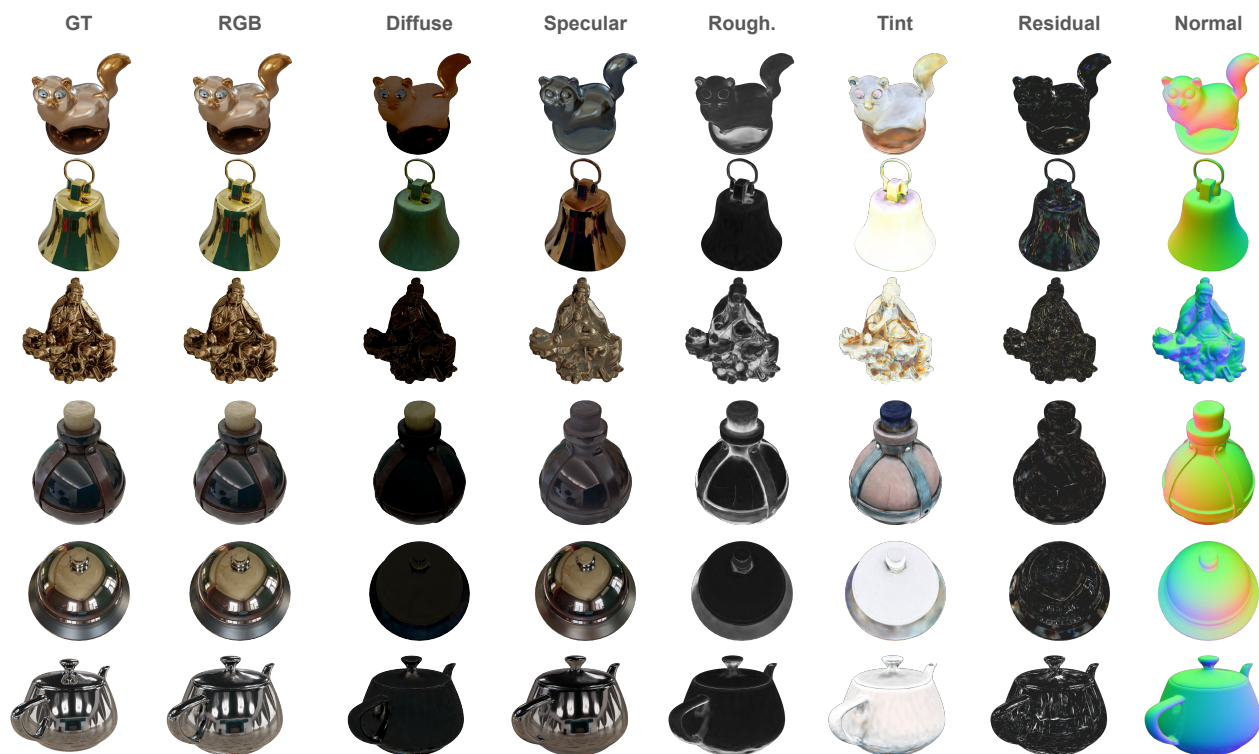


Figure 10. Outputs of our model including diffuse, specular and residual colors, material properties, as well as surface normals for scenes from the Glossy Synthetic [19]. The residuals are amplified for visualization purposes.

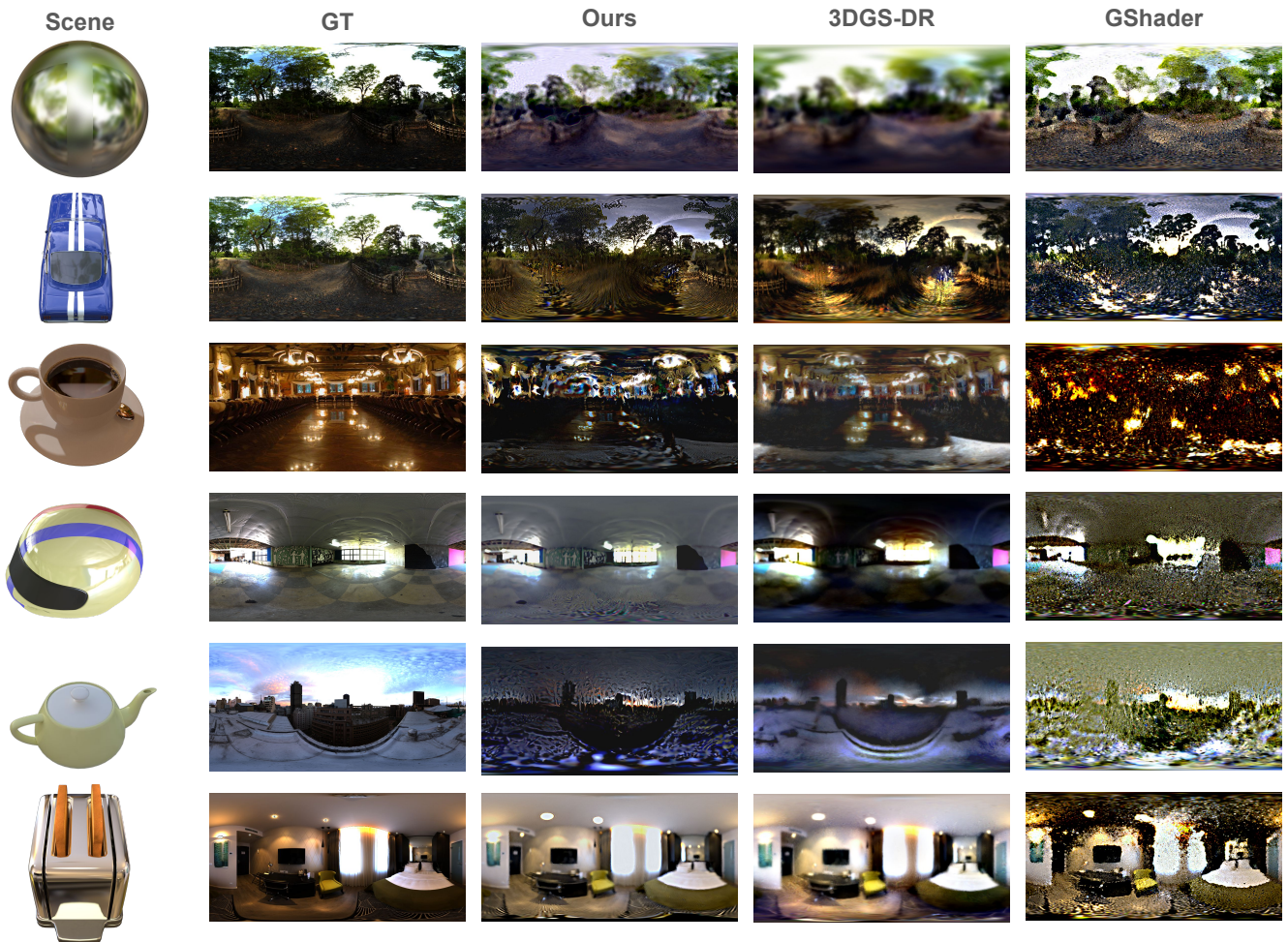


Figure 11. Estimated environment maps on the Shiny Synthetic dataset [33] recovered by our method RGS-DR, 3DGS-DR [16] and GaussianShader [12]. In most cases, we recover sharper details with less blurriness or noise than the competing methods.

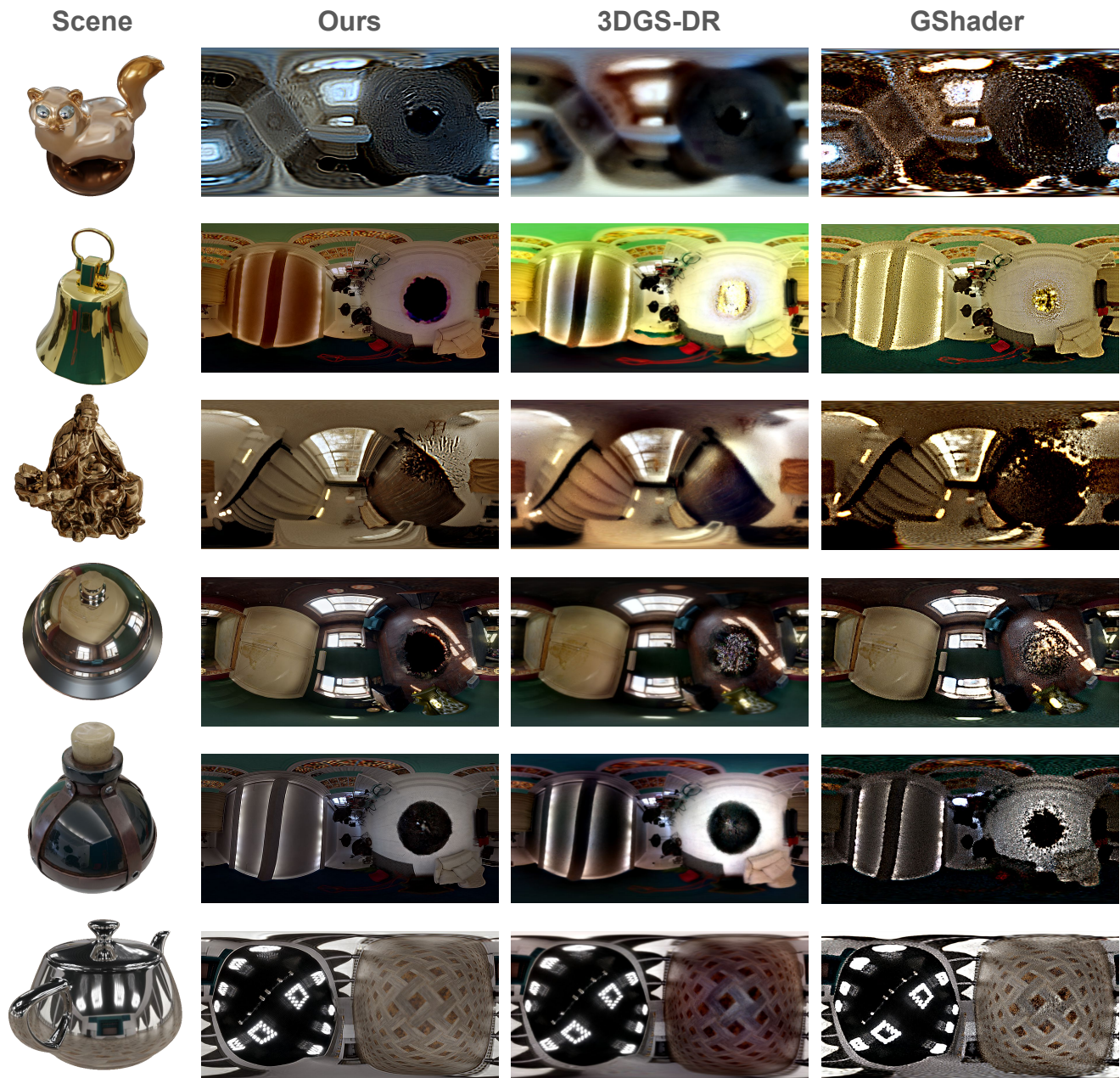


Figure 12. Estimated environment maps on the Glossy Synthetic dataset [19] recovered by our method RGS-DR, 3DGS-DR [16] and GaussianShader [12]. In most cases, we recover sharper details with less blurriness or noise than the competing methods.

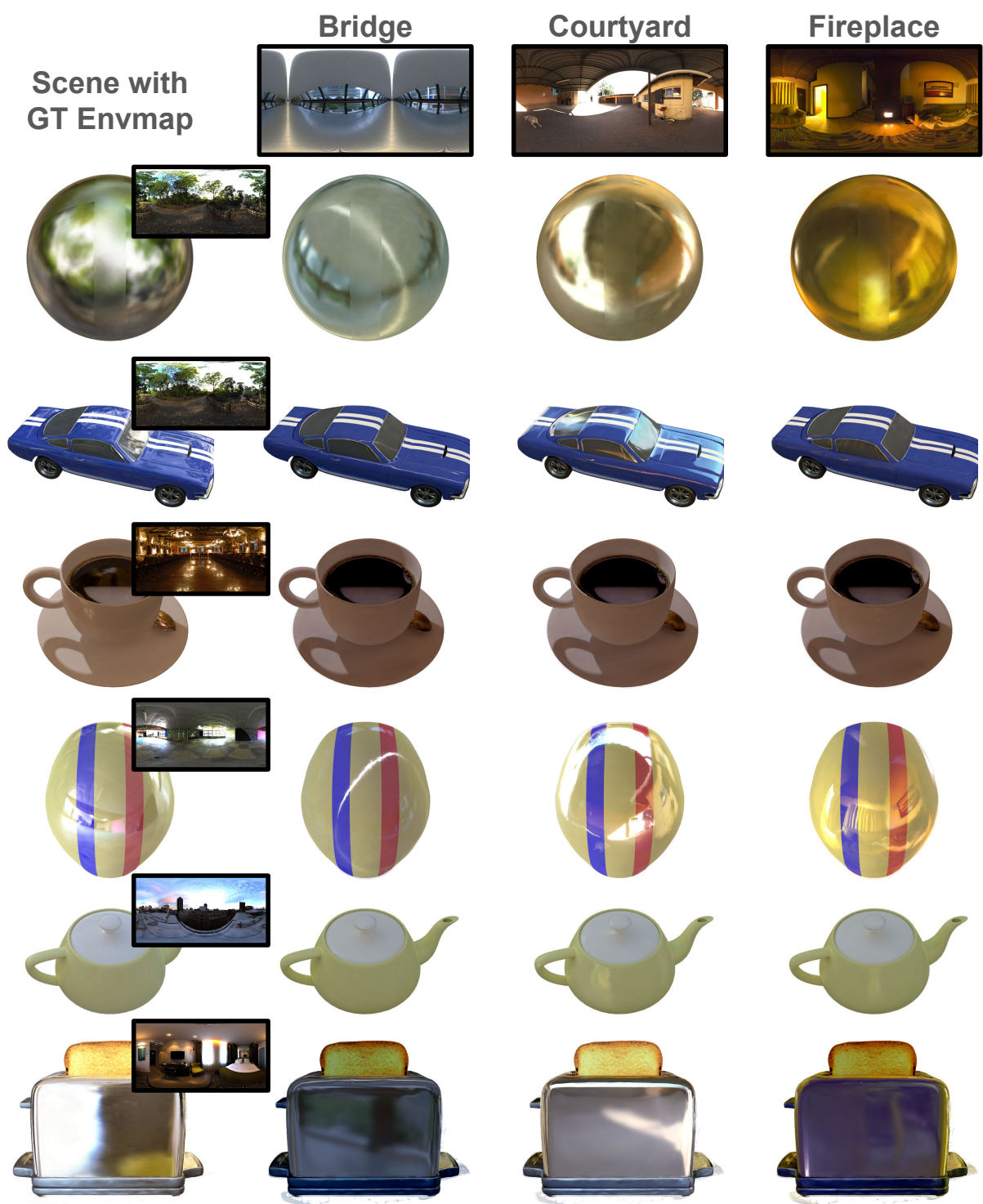


Figure 13. Relighting results on the entire set of scenes of the Shiny Synthetic dataset [33]. High-quality and sharp reflections and specular highlights are observed in all scenes and especially the more glossy scenes, showcasing the successful estimate of scene properties. From left to right, we present the optimized scenes with their original environment illumination, followed by three relighting experiments per scene using three distinct environment maps, namely bridge, courtyard, and fireplace.

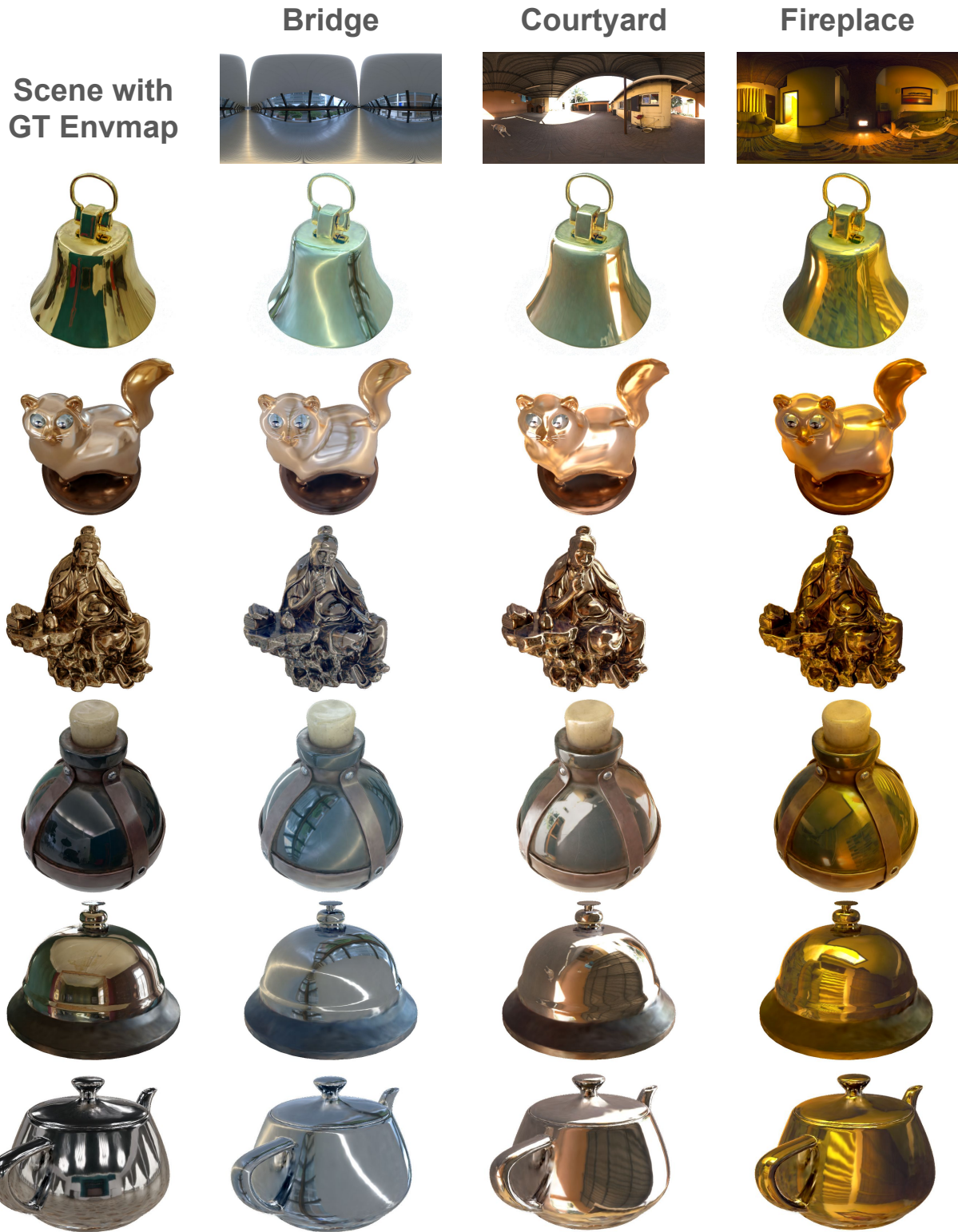


Figure 14. Relighting results on the entire set of examined scenes from the Glossy Synthetic dataset [19]. High-quality and sharp reflections and specular highlights are observed in all scenes and especially the more glossy scenes, showcasing the successful estimate of scene properties. From left to right, we present the optimized scenes with their original environment illumination, followed by three relighting experiments per scene using three distinct environment maps, namely bridge, courtyard, and fireplace.

Supplementary Material:

RGS-DR: Reflective Gaussian Surfels with Deferred Rendering for Shiny Objects

Georgios Kouros Minye Wu Tinne Tuytelaars
 KU Leuven

{georgios.kouros,minye.wu,tinne.tuytelaars}@esat.kuleuven.be

In this supplementary material, we provide additional qualitative results to showcase the contributions of our proposed methodology, including model outputs and scene decompositions, estimated environment maps, relightings. Last but not least, we provide a video demonstration of our method with smooth animations of rendered scenes showcasing the capabilities of our method for reconstruction, relighting and scene editing. We compare our results with the corresponding results of 3DGS-DR [16] and Gaussian Shader [12] and demonstrate the superiority of our approach.

1. Model Outputs and Scene Properties

In Fig. 1 and Fig. 2, we present the outputs and scene decompositions of our method on the Shiny Synthetic [33] dataset and the Glossy Synthetic [19] dataset, respectively. From left to right, we present the ground-truth color, our method’s reconstructed appearance, diffuse color, specular color, roughness, specular tint, residual color and surface normals. These results demonstrated the capability of our method to effectively disentangle the geometry, material properties and illumination during inverse rendering thus facilitating high quality reconstruction, relighting, and scene editing of reflective surfaces.

2. Recovered Environment Maps

In Fig. 3 and Fig 4 we show additional results on estimated environment maps for all evaluated scenes on the Shiny Synthetic [33] and Glossy Synthetic [19] datasets. As evident, our method consistently outperforms 3DGS-DR [16] and GaussianShader [12], on the shinier scenes e.g. car, helmet and the entire Glossy Synthetic scenes, while being competitive on the rest. In general, we recover sharper details of the environment illumination with less artifacts or blurring, although we note a drop in quality for the rougher objects, e.g. coffee and teapot from the Shiny Synthetic dataset.

3. Additional Relighting Results

In Fig. 5 and Fig. 6, we demonstrate the relighting capabilities of our method by applying three novel environment illuminations on all examined scenes from the two synthetic datasets. We observe high-quality relighted reconstructions with preserved underlying geometry and material properties, while under different lighting.

4. Supplementary Video

In the supplementary video, we demonstrate the outputs of our method using smooth animations of reconstructed scenes. First, we showcase the decomposition of a scene into its material properties and light components (diffuse, specular, residual), as well as the underlying geometry (surface normals). Then we show side-by-side comparisons of rendered objects by our method versus 3DGS-DR [16] and GaussianShader [12]. Our method clearly outperforms both methods on geometry estimation thanks to the utilized 2D Gaussian surfels, showcasing less artifacts, smoother geometry, better appearance reconstruction than GaussianShader and usually on par or better reconstruction than 3DGS-DR. Then we present some additional relighting results before ending the video with more high-quality rendered animations of glossy objects. The video can be watched at the following URL: https://drive.google.com/file/d/1kpqeQsaXWb5cowzXnJSsV_OqOu69zT8G/view?usp=sharing

5. Limitations

Our results reveal several limitations. First, the assumption of deferred shading that each pixel corresponds to the nearest opaque surface prevents proper handling of transparent or refractive objects — a shortcoming that might be overcome by combining deferred rendering for opaque surfaces with forward rendering for transparent ones. Second, the absence of multi-bounce ray tracing and explicit visibility reasoning hinders our ability to manage interreflections and

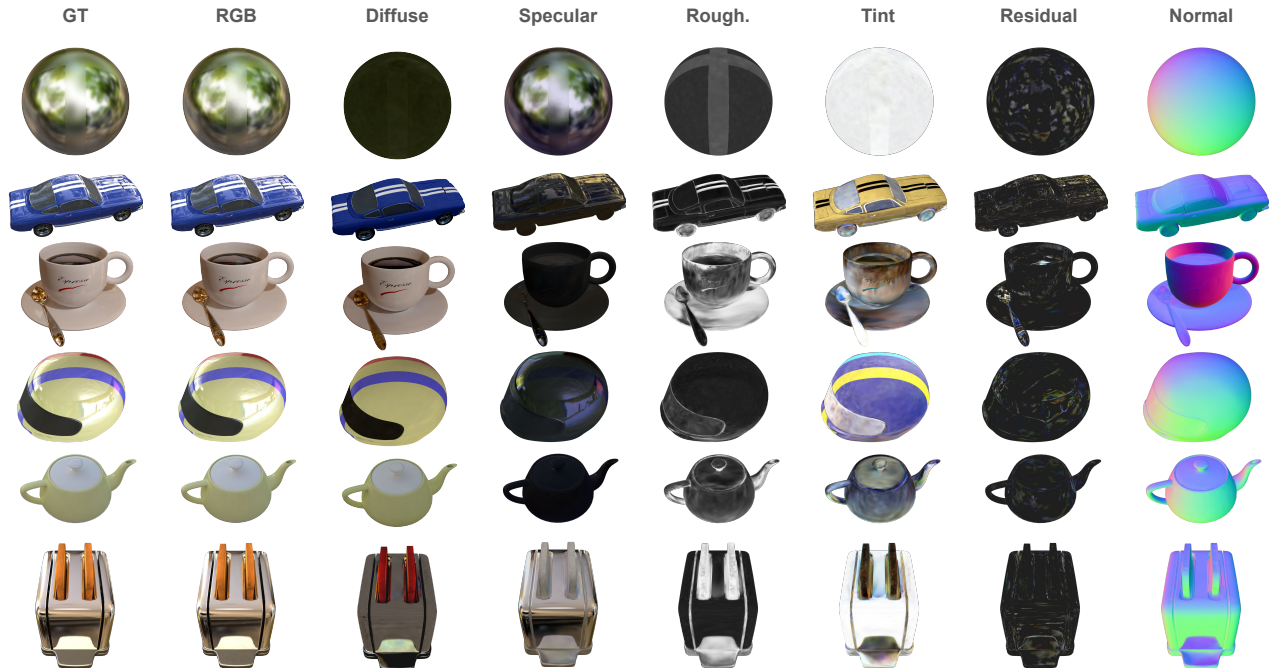


Figure 1. Outputs of our model including diffuse, specular and residual colors, material properties, as well as surface normals for scenes from the Shiny Synthetic [33]. The residuals are amplified for visualization purposes.

shadows, adversely affecting performance on the coffee and teapot scenes of the Shiny Synthetic dataset [33]. Third, the residual pass is only used for refining the model for novel view synthesis without any benefit to the geometry estimation or relighting tasks. Ideally, the residual should be used to compensate for interreflections and other poorly modelled effects during optimization to alleviate geometry distortions as well. Finally, the approach is not yet applicable to unbounded scenes, requiring either ray contraction [1] and a bounding volume around the foreground object [16] to mitigate interference from sparsely observed background features. Such sparsely seen features in the background are perceived as view-dependent effects that result in erroneous reflective surfels. At the moment, this can only be addressed by using a bounding volume that penalizes low roughness of all surfels outside the bounding volume.

References

- [1] Jonathan T. Barron, Ben Mildenhall, Dor Verbin, Pratul P. Srinivasan, and Peter Hedman. Mip-nerf 360: Unbounded anti-aliased neural radiance fields. *CVPR*, 2022. 2
- [2] Sai Bi, Zexiang Xu, Kalyan Sunkavalli, Miloš Hašan, Yannick Hold-Geoffroy, David Kriegman, and Ravi Ramamoorthi. Deep reflectance volumes: Relightable reconstructions from multi-view photometric images. In *European Conference on Computer Vision (ECCV)*, page 294–311, Berlin, Heidelberg, 2020. Springer-Verlag.
- [3] Mark Boss, Raphael Braun, Varun Jampani, Jonathan T. Barron, Ce Liu, and Hendrik P.A. Lensch. NerD: Neural reflectance decomposition from image collections. In *IEEE International Conference on Computer Vision (ICCV)*, 2021.
- [4] Mark Boss, Varun Jampani, Raphael Braun, Ce Liu, Jonathan T. Barron, and Hendrik P.A. Lensch. Neural-pil: Neural pre-integrated lighting for reflectance decomposition. In *Advances in Neural Information Processing Systems (NeurIPS)*, 2021.
- [5] Brian Chao, Hung-Yu Tseng, Lorenzo Porzi, Chen Gao, Tuotuo Li, Qinbo Li, Ayush Saraf, Jia-Bin Huang, Johannes Kopf, Gordon Wetzstein, et al. Textured gaussians for enhanced 3d scene appearance modeling. *arXiv preprint arXiv:2411.18625*, 2024.
- [6] Danpeng Chen, Hai Li, Weicai Ye, Yifan Wang, Weijian Xie, Shangjin Zhai, Nan Wang, Haomin Liu, Hujun Bao, and Guofeng Zhang. Pgsr: Planar-based gaussian splatting for efficient and high-fidelity surface reconstruction. *IEEE Transactions on Visualization and Computer Graphics*, 2024.
- [7] Robert L Cook and Kenneth E. Torrance. A reflectance model for computer graphics. *ACM Transactions on Graphics (ToG)*, 1(1):7–24, 1982.
- [8] Michael Deering, Stephanie Winner, Bic Schediwy, Chris Duffy, and Neil Hunt. The triangle processor and normal vector shader: a vlsi system for high performance graphics. *Acm siggraph computer graphics*, 22(4):21–30, 1988.
- [9] Yue Fan, Ivan Skorokhodov, Oleg Voynov, Savva Ignatyev, Evgeny Burnaev, Peter Wonka, and Yiqun Wang. Factored-nerf: Reconstructing surfaces, illumination, and materials of possibly glossy objects, 2023.
- [10] Duan Gao, Guojun Chen, Yue Dong, Pieter Peers, Kun Xu,



Figure 2. Outputs of our model including diffuse, specular and residual colors, material properties, as well as surface normals for scenes from the Glossy Synthetic [19]. The residuals are amplified for visualization purposes.

- and Xin Tong. Deferred neural lighting: free-viewpoint re-lighting from unstructured photographs. *ACM Transactions on Graphics (TOG)*, 39(6):258, 2020.
- [11] Binbin Huang, Zehao Yu, Anpei Chen, Andreas Geiger, and Shenghua Gao. 2d gaussian splatting for geometrically accurate radiance fields. In *SIGGRAPH 2024 Conference Papers*. Association for Computing Machinery, 2024.
- [12] Yingwenqi Jiang, Jiadong Tu, Yuan Liu, Xifeng Gao, Xiaoxiao Long, Wenping Wang, and Yuexin Ma. Gaussian-shader: 3d gaussian splatting with shading functions for reflective surfaces. In *Proceedings of the IEEE/CVF Conference on Computer Vision and Pattern Recognition (CVPR)*, pages 5322–5332, 2024. 1, 4, 5
- [13] Haian Jin, Isabella Liu, Peijia Xu, Xiaoshuai Zhang, Songfang Han, Sai Bi, Xiaowei Zhou, Zexiang Xu, and Hao Su. Tensoir: Tensorial inverse rendering. In *Proceedings of the IEEE/CVF Conference on Computer Vision and Pattern Recognition (CVPR)*, 2023.
- [14] James T Kajiya. The rendering equation. In *Proceedings of the 13th annual conference on Computer graphics and interactive techniques*, pages 143–150, 1986.
- [15] Bernhard Kerbl, Georgios Kopanas, Thomas Leimkühler, and George Drettakis. 3d gaussian splatting for real-time radiance field rendering. *ACM Transactions on Graphics*, 42(4), 2023.
- [16] Ye Keyang, Hou Qiming, and Zhou Kun. 3d gaussian splatting with deferred reflection. 2024. 1, 2, 4, 5
- [17] Ruofan Liang, Huiting Chen, Chunlin Li, Fan Chen, Selvakumar Panneer, and Nandita Vijaykumar. Envidr: Implicit differentiable renderer with neural environment lighting. In *Proceedings of the IEEE/CVF International Conference on Computer Vision*, pages 79–89, 2023.
- [18] Lingjie Liu, Jiatao Gu, Kyaw Zaw Lin, Tat-Seng Chua, and Christian Theobalt. Neural sparse voxel fields. *NeurIPS*, 2020.
- [19] Yuan Liu, Peng Wang, Cheng Lin, Xiaoxiao Long, Jiepeng Wang, Lingjie Liu, Taku Komura, and Wenping Wang. Nero: Neural geometry and brdf reconstruction of reflective objects from multiview images. *ACM Trans. Graph.*, 42(4), 2023. 1, 3, 5, 8
- [20] Tao Lu, Mulin Yu, Linning Xu, Yuanbo Xiangli, Limin Wang, Dahua Lin, and Bo Dai. Scaffold-gs: Structured 3d gaussians for view-adaptive rendering. In *Proceedings of the IEEE/CVF Conference on Computer Vision and Pattern Recognition*, pages 20654–20664, 2024.
- [21] Alexander Mai, Dor Verbin, Falko Kuester, and Sara Fridovich-Keil. Neural microfacet fields for inverse rendering. In *Proceedings of the IEEE/CVF International Conference on Computer Vision*, pages 408–418, 2023.
- [22] Ben Mildenhall, Pratul P. Srinivasan, Matthew Tancik, Jonathan T. Barron, Ravi Ramamoorthi, and Ren Ng. Nerf:

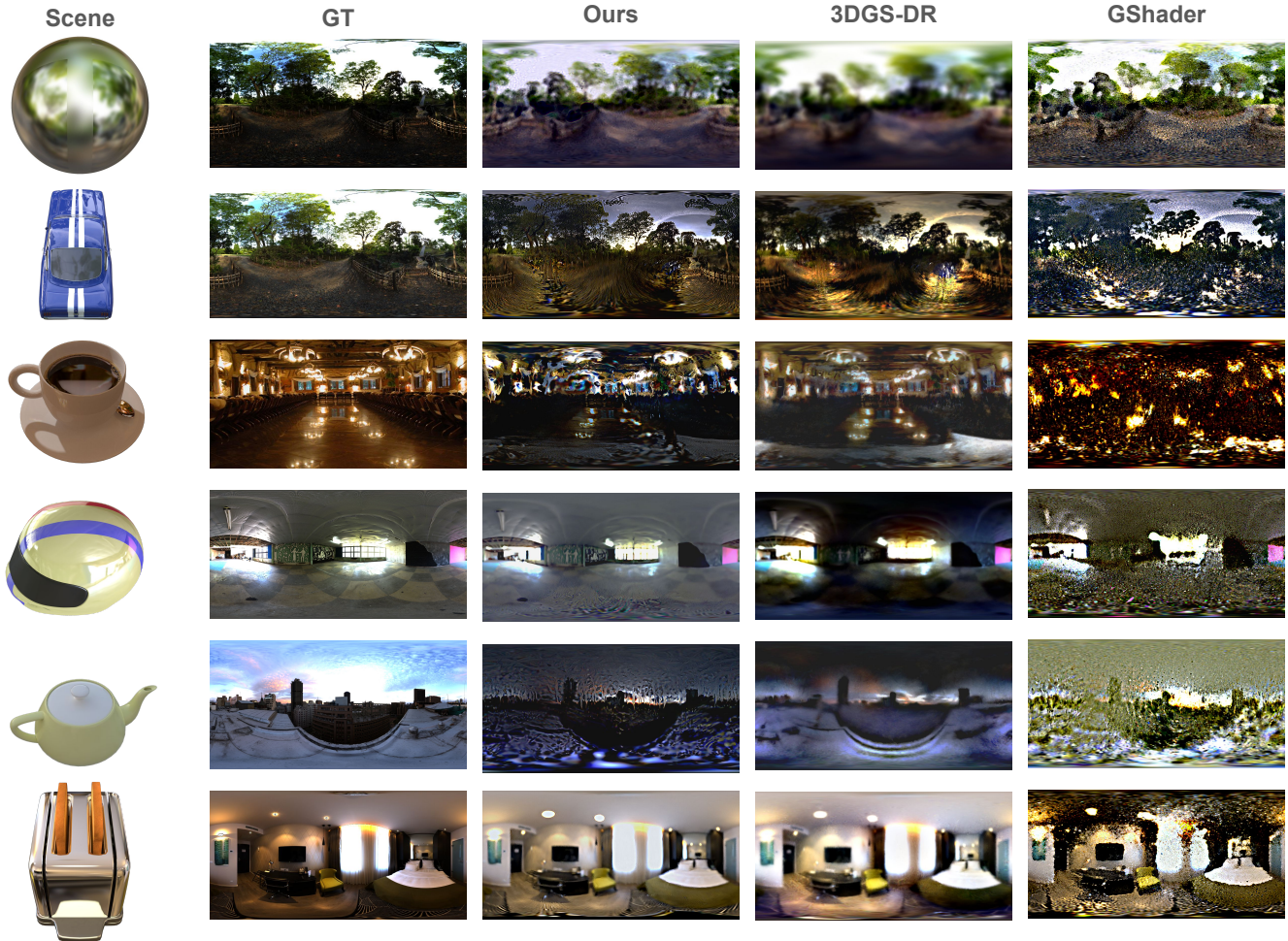


Figure 3. Estimated environment maps on the Shiny Synthetic dataset [33] recovered by our method RGS-DR, 3DGS-DR [16] and GaussianShader [12]. In most cases, we recover sharper details with less blurriness or noise than the competing methods.

- Representing scenes as neural radiance fields for view synthesis. In *ECCV*, 2020.
- [23] Ben Mildenhall, Pratul P Srinivasan, Matthew Tancik, Jonathan T Barron, Ravi Ramamoorthi, and Ren Ng. Nerf: Representing scenes as neural radiance fields for view synthesis. *Communications of the ACM*, 65(1):99–106, 2021.
- [24] Thomas Müller, Alex Evans, Christoph Schied, and Alexander Keller. Instant neural graphics primitives with a multi-resolution hash encoding. *ACM Trans. Graph.*, 41(4):102:1–102:15, 2022.
- [25] Hanspeter Pfister, Matthias Zwicker, Jeroen Van Baar, and Markus Gross. Surfels: Surface elements as rendering primitives. In *Proceedings of the 27th annual conference on Computer graphics and interactive techniques*, pages 335–342, 2000.
- [26] Kerui Ren, Lihan Jiang, Tao Lu, Mulin Yu, Linning Xu, Zhangkai Ni, and Bo Dai. Octree-gs: Towards consistent real-time rendering with lod-structured 3d gaussians. *arXiv preprint arXiv:2403.17898*, 2024.
- [27] Samuel Rota Bulò, Lorenzo Porzi, and Peter Kotschieder. Revising densification in gaussian splatting. In *European Conference on Computer Vision*, pages 347–362. Springer, 2024.
- [28] Sara Fridovich-Keil and Alex Yu, Matthew Tancik, Qinhong Chen, Benjamin Recht, and Angjoo Kanazawa. Plenoxels: Radiance fields without neural networks. In *CVPR*, 2022.
- [29] Pratul P. Srinivasan, Boyang Deng, Xiuming Zhang, Matthew Tancik, Ben Mildenhall, and Jonathan T. Barron. Nerv: Neural reflectance and visibility fields for relighting and view synthesis. In *CVPR*, 2021.
- [30] Cheng Sun, Min Sun, and Hwann-Tzong Chen. Direct voxel grid optimization: Super-fast convergence for radiance fields reconstruction. In *CVPR*, 2022.
- [31] Cheng Sun, Min Sun, and Hwann-Tzong Chen. Improved direct voxel grid optimization for radiance fields reconstruction, 2022.
- [32] Zhe Jun Tang and Tat-Jen Cham. 3igs: Factorised tensorial illumination for 3d gaussian splatting. In *European Conference on Computer Vision*, pages 143–159. Springer, 2024.
- [33] Dor Verbin, Peter Hedman, Ben Mildenhall, Todd Zickler,

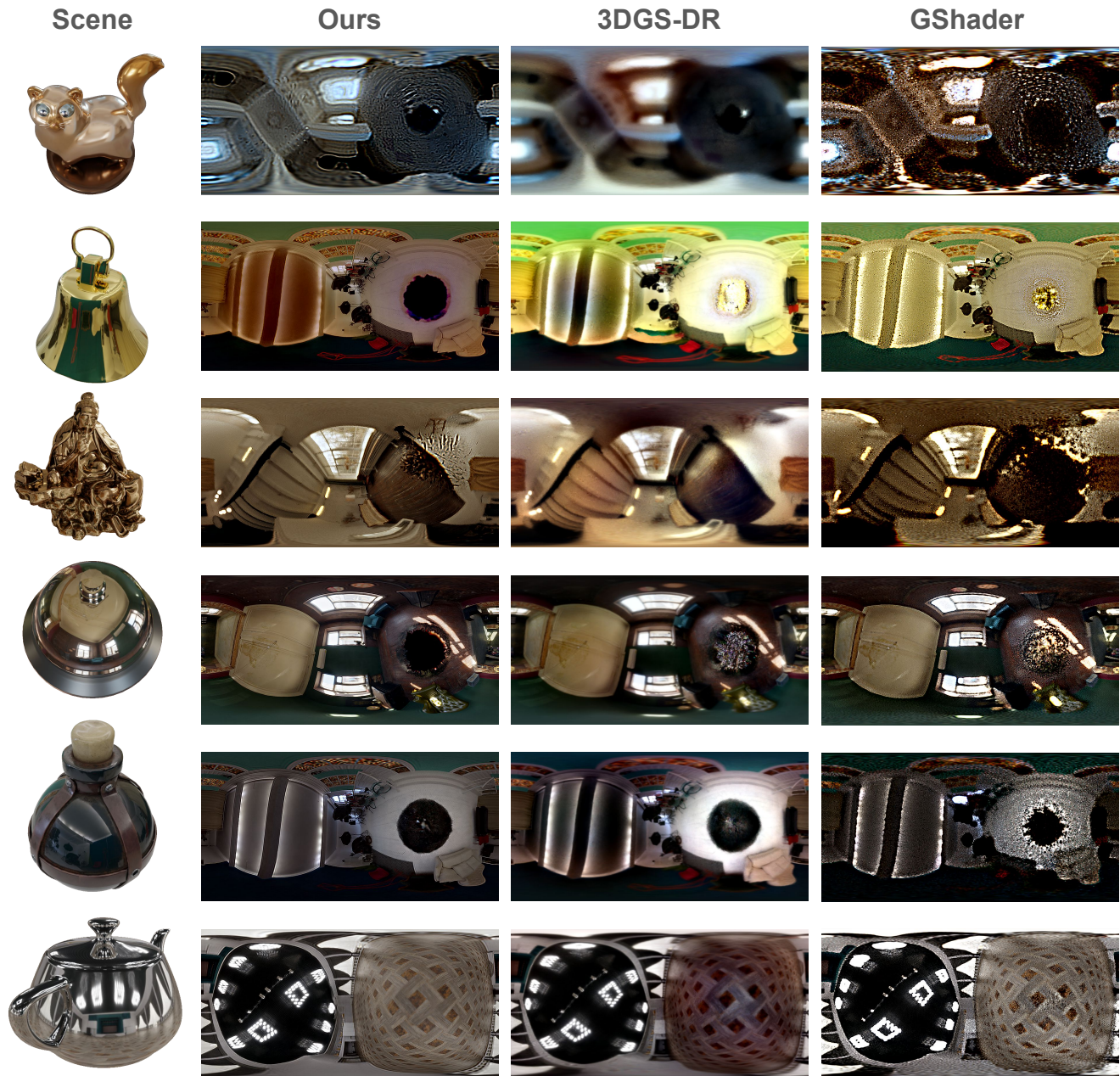


Figure 4. Estimated environment maps on the Glossy Synthetic dataset [19] recovered by our method RGS-DR, 3DGS-DR [16] and GaussianShader [12]. In most cases, we recover sharper details with less blurriness or noise than the competing methods.

Jonathan T. Barron, and Pratul P. Srinivasan. Ref-NeRF: Structured view-dependent appearance for neural radiance fields. *CVPR*, 2022. 1, 2, 4, 6

[34] Bruce Walter, Stephen R Marschner, Hongsong Li, and Kenneth E Torrance. Microfacet models for refraction through rough surfaces. *Rendering techniques*, 2007:18th, 2007.

[35] Tong Wu, Jia-Mu Sun, Yu-Kun Lai, Yuewen Ma, Leif Kobbelt, and Lin Gao. Deferredrgs: Decoupled and editable gaussian splatting with deferred shading. *arXiv preprint*

arXiv:2404.09412, 2024.

[36] Zehao Yu, Anpei Chen, Binbin Huang, Torsten Sattler, and Andreas Geiger. Mip-splatting: Alias-free 3d gaussian splatting. In *Proceedings of the IEEE/CVF conference on computer vision and pattern recognition*, pages 19447–19456, 2024.

[37] Kai Zhang, Fujun Luan, Qianqian Wang, Kavita Bala, and Noah Snavely. Physg: Inverse rendering with spherical gaussians for physics-based material editing and relighting. In

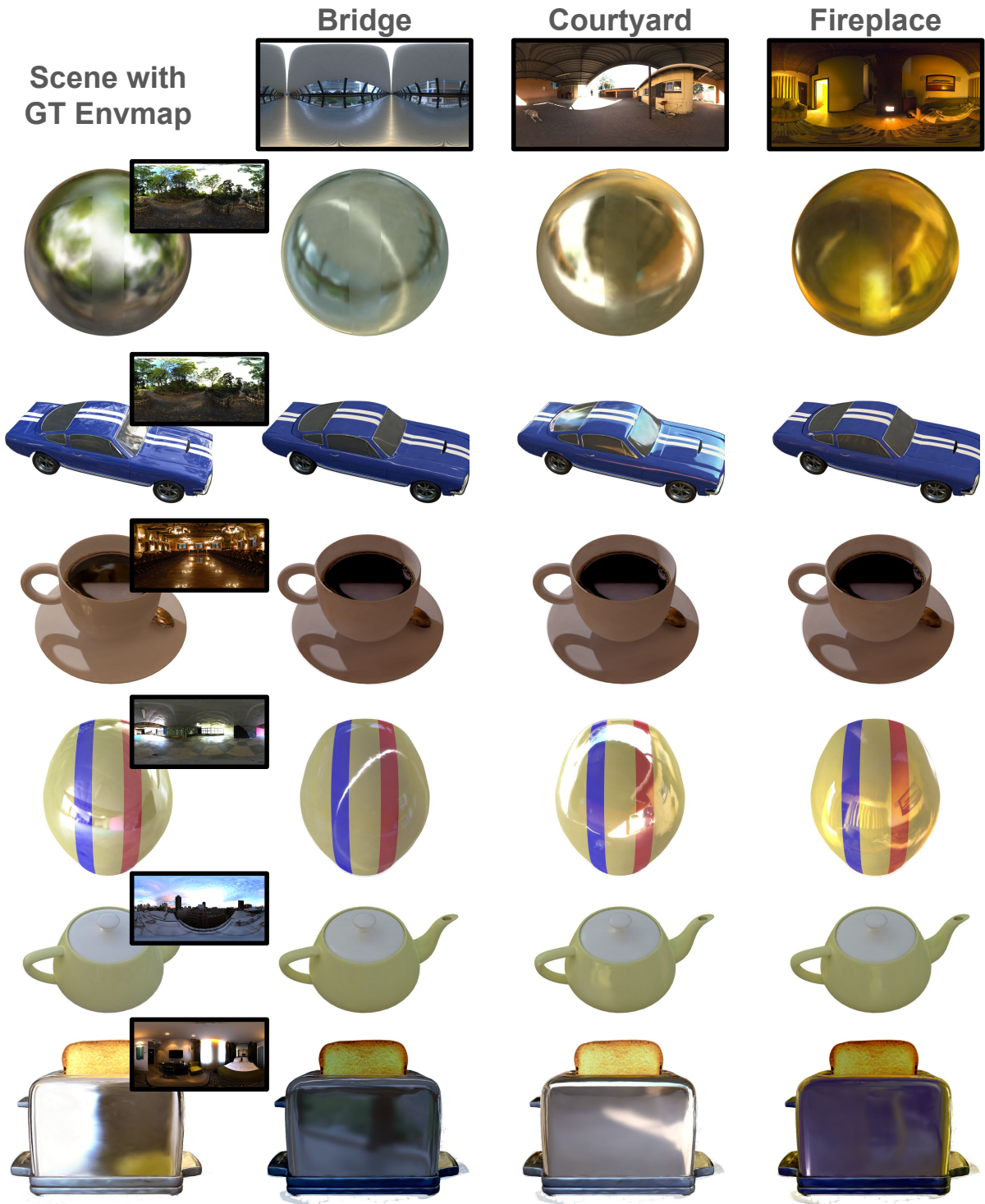


Figure 5. Relighting results on the entire set of scenes of the Shiny Synthetic dataset [33]. High-quality and sharp reflections and specular highlights are observed in all scenes and especially the more glossy scenes, showcasing the successful estimate of scene properties. From left to right, we present the optimized scenes with their original environment illumination, followed by three relighting experiments per scene using three distinct environment maps, namely bridge, courtyard, and fireplace.

Proceedings of the IEEE/CVF Conference on Computer Vision and Pattern Recognition, pages 5453–5462, 2021.

- [38] Xiuming Zhang, Pratul P. Srinivasan, Boyang Deng, Paul Debevec, William T. Freeman, and Jonathan T. Barron. Ner-factor: neural factorization of shape and reflectance under an unknown illumination. *ACM Trans. Graph.*, 40(6), 2021.
- [39] Youjia Zhang, Anpei Chen, Yumin Wan, Zikai Song, Junqing Yu, Yawei Luo, and Wei Yang. Ref-gs: Directional factorization for 2d gaussian splatting. *arXiv preprint arXiv:2412.00905*, 2024.
- [40] Zheng Zhang, Wenbo Hu, Yixing Lao, Tong He, and Hengshuang Zhao. Pixel-gs: Density control with pixel-aware gradient for 3d gaussian splatting. In *European Conference on Computer Vision*, pages 326–342. Springer, 2024.
- [41] Zuo-Liang Zhu, Beibei Wang, and Jian Yang. Gs-ror: 3d gaussian splatting for reflective object relighting via sdf priors. *arXiv preprint arXiv:2406.18544*, 2024.



Figure 6. Relighting results on the entire set of examined scenes from the Glossy Synthetic dataset [19]. High-quality and sharp reflections and specular highlights are observed in all scenes and especially the more glossy scenes, showcasing the successful estimate of scene properties. From left to right, we present the optimized scenes with their original environment illumination, followed by three relighting experiments per scene using three distinct environment maps, namely bridge, courtyard, and fireplace.